

Geometric quenches in quasisordered lattice systems

Ravi Kumar¹ and Ranjan Modak²

¹*Department of Physics, Indian Institute of Technology (Banaras Hindu University), Varanasi 221005, India*

²*Department of Physics, Indian Institute of Technology Tirupati, Tirupati 517506, India*



(Received 10 March 2022; revised 6 May 2022; accepted 26 May 2022; published 9 June 2022)

While global quantum quench has been extensively used in the literature to understand the localization-delocalization transition for the one-dimensional quantum spin chain, the effect of geometric quench (which corresponds to a sudden change of the geometry of the chain) in the context of such transitions is yet to be well understood. In this work, we investigate the effect of geometric quench in the Aubry-André model, which supports localization-delocalization transition even in one dimension. We study the spreading of the entanglement and the site occupation with time and find many interesting features that can be used to characterize localization-delocalization transition. We observe that geometric quench causes a power-law type growth of the entanglement entropy in the delocalized phase in contrast to the linear growth which is found in the global quench studies. We also find that the saturation values in the many-body localized (MBL) phase obey area law in contrast to the usual volume law, which is a signature feature of the MBL phase in the context of global quench. This area law can also be understood from the long time site-occupation profile in the MBL phase.

DOI: [10.1103/PhysRevB.105.224202](https://doi.org/10.1103/PhysRevB.105.224202)

I. INTRODUCTION

In one dimension, any arbitrary weak amount of disorder is sufficient to localize all eigenstates of a noninteracting system. This phenomenon is famously known as Anderson localization [1,2]. The question of how this picture is modified by interactions remained unclear for a very long time. However, relatively recently, Basko, Aleiner, and Altshuler have argued that an interacting many-body system can undergo a so-called many-body localization (MBL) transition in the presence of quenched disorder [3]. There has been a plethora of work in this direction in the past decade to understand the nature of this phase transition both theoretically [4–14] and experimentally as well [15–17]. The MBL transition is rather unique in contrast to more conventional quantum phase transitions. This is not a transition in the ground state; instead, the MBL transition involves the localization of highly excited states of a many-body system with finite energy density. Also, this MBL phase is of fundamental interest in the context of statistical mechanics. Local subsystems of a generic interacting many-body system are expected to equilibrate with their surroundings and that has led to the so-called eigenstate thermalization hypothesis (ETH), which states that individual eigenstates of the interacting system encode thermal distributions of local quantities [18–20]. However, the many-body localized phase is an exception, in which the individual eigenstates fail to obey ETH and the notion of ergodicity breaks down [21,22].

Most of the out-of-equilibrium studies of localization-delocalization transition involve the so-called quantum quench, in which a system is initially prepared in the ground state of a many-body quantum Hamiltonian, and a nontrivial unitary dynamics is then induced by changing instantaneously (i.e., quenching) one (or many) control parameters. Depend-

ing on whether this change happens locally or in the whole system, the quench falls into the class of local or global quenches, respectively. One uses universal features of different diagnostics, e.g., entanglement entropy, out of time correlators (OTOC) to distinguish between different phases of the systems [23–28].

In our work, we focus on a situation that is intermediate between a local and a global quench. We consider the real-time dynamics following an instantaneous change of the geometry or the size of the system, the so-called geometric quench [29–32]. More specifically, we prepare an initial state, which is say the ground state of a lattice Hamiltonian of length L_A , then study unitary dynamics under the same lattice Hamiltonian of length L , where $L > L_A$. The question we are addressing here is whether one can use this geometric quench as a probe to detect localization-delocalization transitions. Thanks to extraordinary advancements of ultracold gas experiments, this kind of sudden expansion of lattice size or traps has been realized in recent days [33,34].

Given that a noninteracting one-dimensional system of fermions in the presence of a true disorder does not show any localization-delocalization transition, the Aubry-André (AA) Hamiltonian [35] is one of the best suited Hamiltonians in order to investigate the effect of geometric quench in the localization-delocalization transition. Instead of pure randomness, this model has the incommensurate on-site potential, which drives a system in the localized phase, and the localization-delocalization transition occurs for a finite incommensurate potential amplitude in contrast to the usual Anderson localization in one dimension, which requires only an infinitesimal disorder strength to localize all states. One can also explore the MBL transition introducing the interaction in this model [36].

In our study, we investigate the effect of geometric quench in the Aubry-André model. We have used the spreading of the entanglement and the site-occupation with time as two tools to characterize localization-delocalization transition. Our main two results are the following. (1) We have observed that geometric quench causes a power-law type growth of the entanglement entropy in the delocalized phase in contrast to the linear growth, which is found in the global quench studies. (2) The saturation values in the many-body localized (MBL) phase obey area law in contrast to the usual volume law which is a signature feature of the MBL phase in the context of global quench [37]. This area law feature can also be well understood from the site-occupation profile in the MBL phase.

The paper is organized as follows. In Sec. II, we introduce the model and protocols. Next, we discuss the characteristics of the site-occupation profile in Sec. III. In Sec. IV, we investigate entanglement dynamics followed by geometric quench. Finally, in Sec. V, we summarize our results.

II. MODEL AND PROTOCOLS

We study a system of fermions in a one-dimensional lattice of size L , which is described by the following Hamiltonian:

$$\hat{H} = - \sum_{i=1}^{L-1} (\hat{c}_i^\dagger \hat{c}_{i+1} + \text{H.c.}) + 2h \sum_{i=1}^L \cos(2\pi\alpha i + \phi) \hat{n}_i + V \sum_i \hat{n}_i \hat{n}_{i+1}, \quad (1)$$

where \hat{c}_i^\dagger (\hat{c}_i) is the fermionic creation (annihilation) operator at site i , $\hat{n}_i = \hat{c}_i^\dagger \hat{c}_i$ is the number operator, and α is an irrational number. Without loss of any generality, we choose $\alpha = \frac{\sqrt{5}-1}{2}$, and ϕ is a random number chosen between $[0, 2\pi]$. We average over ϕ for all the calculations presented in this work to obtain better statistics. In the absence of interaction, i.e., $V = 0$, the Hamiltonian \hat{H} is known as the Aubry-André (AA) model. It supports a delocalization-localization transition as one tunes h . In the thermodynamic limit, $h = 1$ corresponds to the transition point [35].

Given that we wanted to investigate the effect of geometric quench in these systems, we do the following quench protocols. First, we prepare the initial state as a ground state of the Hamiltonian \hat{H} in a one-dimensional lattice of size $L_A < L$ and keep the $(L - L_A)$ sites completely empty. For all our calculations, we fixed the total number of fermions as $N = L_A/2$ and $L_A = L/2$. Then we let the state evolve under the unitary evolution of the Hamiltonian \hat{H} , which is supported in a one-dimensional lattice of size L . This quench protocol is different than the local quench [38–41], where the initial state is obtained by “gluing” together with two identical copies of the ground state, i.e., $|\psi(t=0)\rangle = |GS\rangle_{L_A} \otimes |GS\rangle_{(L-L_A)}$. On the other hand, in our case, the initial state is chosen to be $|\psi(t=0)\rangle = |GS\rangle_{L_A} \otimes |0\rangle_{(L-L_A)}$. For $V = 0$, all the calculations are done using the on-body density matrix approach [42], while for the interacting case we use the finite time density matrix renormalization group (tDMRG) technique [43–46] to obtain all the results. Some of the data displayed in the main text are obtained using the tDMRG algorithm, as implemented in the ITensor Julia library [47].

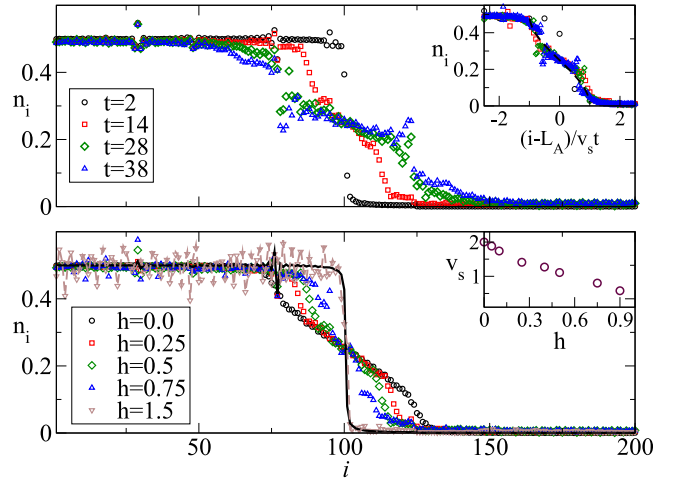


FIG. 1. (Upper panel) Variation of the site occupation for different time for $h = 0.5$, and $L = 2L_A = 200$. Inset shows the data collapse for the data for different times as we rescale the x axes with $(i - L_A)/v_s t$ and the dashed line represents $n_i = 1/4 - (1/2\pi) \sin^{-1}[(i - L_A)/v_s t]$, where v_s is the fitting parameter. (Lower panel) Variation of n_i for different values of h for fixed time $t = 14$. Solid and dashed lines correspond to the site occupation for $t = 0$ for $h = 0.25$ and $h = 1.5$, respectively. Inset shows the variation of the fitting parameter v_s with h .

III. SITE OCCUPATION

In this section, we discuss the real-time dynamics of the site occupation $n_i = \langle \hat{n}_i \rangle$ subject to the tuning of disorder strength (h) and the interaction (V) after the geometric quench. First, we prepare the initial state to be a ground state of a Hamiltonian (1) on a lattice of size $L/2$. Then we attach an empty lattice of size $L/2$ with it. Hence the site occupation has a domain wall profile in the beginning. Then the site occupation wave front propagates with a velocity $v_s(V, h)$ (function of disorder strength and the interaction) for $t > 0$.

We first focus on the noninteracting case, i.e., $V = 0$. Figure 1 (upper panel) shows the evolution of site occupation $n_i = \langle \hat{n}_i(t) \rangle$ at different time steps for $h = 0.5$. Given that, for $h = 0.5$, the Hamiltonian (1) remains in the delocalized phase, one expects that the wave front would propagate towards the boundary of the lattice; that is precisely what is observed in Fig. 1. The next question one should ask is how does one evaluate the wave front propagation velocity v_s ? For that we use the ansatz, i.e., $\langle n_i(t) \rangle = 1/4 - (1/2\pi) \sin^{-1}[(i - L_A)/v_s t]$, which can be obtained analytically using a semiclassical reasoning that was also applied in Refs. [48,49] for $h = 0$. We also get a remarkable data collapse for $n_i = \langle \hat{n}_i \rangle$ versus rescaled variable $(i - L_A)/v_s t$ as shown in the inset of Fig. 1.

Next, we discuss the effect of disorder strength on the propagation of the site occupation wave front. As we increase the disorder strength (h), the velocity of the wave front starts decreasing and, finally, the wave front almost gets frozen as we cross the transition point, i.e., $h = 1$ as shown in Fig. 1 (lower panel). Inset shows the variation of v_s with h . Now we focus on the effect of interactions. Once we switch on the interaction, we observe melting of the domain wall in the site occupation profile similar to the one observed earlier for

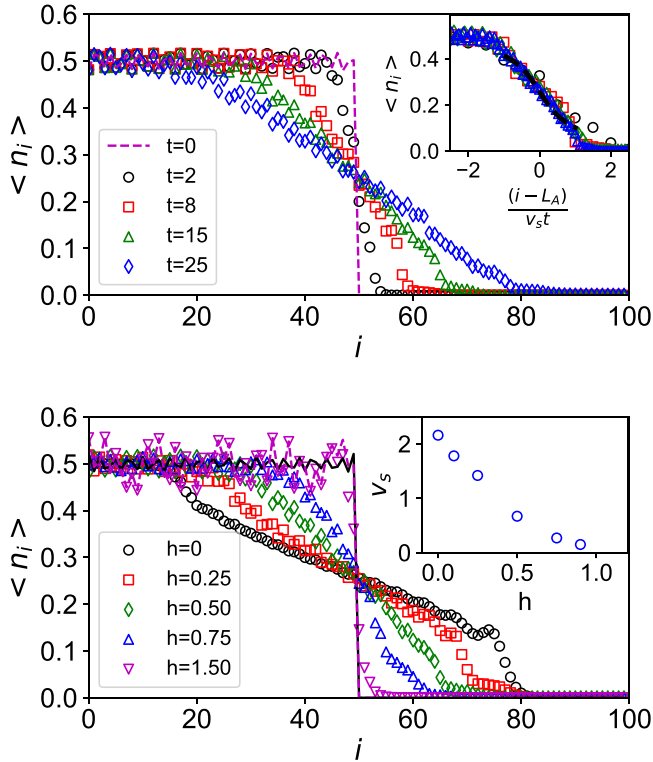


FIG. 2. (Upper panel) Variation of the site occupation for different time for $h = 0.5$, $V = 0.5$, and $L = 2L_A = 100$. Inset shows the data collapse for the data for different times as we rescale the x axis with $(i - L_A)/v_s t$ and the black dashed line represents $n_i = 1/4 - (1/2\pi) \sin^{-1}[(i - L_A)/v_s t]$, where v_s is the fitting parameter. (Lower panel) Variation of n_i for different values of h for fixed time $t = 15$ for $V = 0.5$. Solid and dashed lines correspond to the site occupation for $t = 0$ for $h = 0.0$ and $h = 1.5$, respectively. Inset shows the variation of the fitting parameter v_s with h .

the noninteracting case. Figure 2 (upper panel) describes the propagation of site occupation wave front at different time steps for $V = 0.5$. Once again we use the same ansatz, i.e., $\langle n_i(t) \rangle = 1/4 - (1/2\pi) \sin^{-1}[(i - L_A)/v_s t]$, to extract the v_s . Figure 2 (lower panel) shows the change in behavior of site occupation profile as a function of h for a given time, i.e., $t = 15$. As expected, with the increase of h , the velocity of the propagating wave front starts decreasing, as shown in the inset of Fig. 2 (lower panel). In order to make the comparison even more clear, we plot the variation of v_s with h in Fig. 3 for different values of interaction strength. We see a general feature with v_s , which dies down as we increase the disorder strength h even for the interacting case. This is due to the effect of the many-body localization effect; as we approach the ergodic-MBL transition point, the site occupation profile hardly changes with time. In order to quantify the change in the site occupation profile with time in the delocalized phase, we use another quantifier, i.e., $\Delta n(t) = \sum_i |n_i(t) - n_i(t = 0)|$. In Fig. 4, we show the variation of $\Delta n(t)$ with t for the noninteracting case for different values of h . We find an initial power-law growth, i.e., $\Delta n \sim t^\gamma$, and then it saturates (apart from some small oscillations). Interestingly this exponent $\gamma \simeq 1$ for $h = 0$, but it decreases as one increases the value of h . In the inset, we also show the long time average of

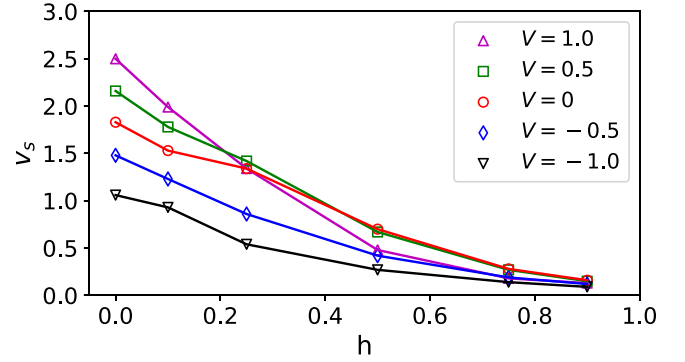


FIG. 3. Variation of the v_s with the disorder strength for $V = 1, 0.5, 0, -0.5, -1$.

Δn , i.e., $\langle \Delta n \rangle = \frac{1}{T_2 - T_1} \int_{T_1}^{T_2} \Delta n dt$ (note that we choose T_1 and T_2 to be large so that Δn at that time window remains in the saturation regime), for different values of h and L and we find that $\langle \Delta n \rangle$ obeys a volume law. Next, we investigate the effect of interactions. As Fig. 5 suggests, we find a similar behavior of $\Delta n(t)$ with t even in the presence of interaction.

However, the exponent γ depends on the interaction and disorder strength, which has been displayed in Fig. 6. While, for $h = 0$, it seems that γ does not depend on interaction strength significantly, for nonzero h , there is a generic trend that the value of γ (for a given h) decreases as the magnitude of interaction strength increases. Due to the limitation of tDMRG simulation, we were unable to reach a very long time; hence the saturation value of Δn cannot be analyzed as one could do it for the noninteracting case.

IV. ENTANGLEMENT DYNAMICS

Next, we investigate the entanglement dynamics. Even though there are many measures to characterize the entanglement, here we focus on probably one of the most

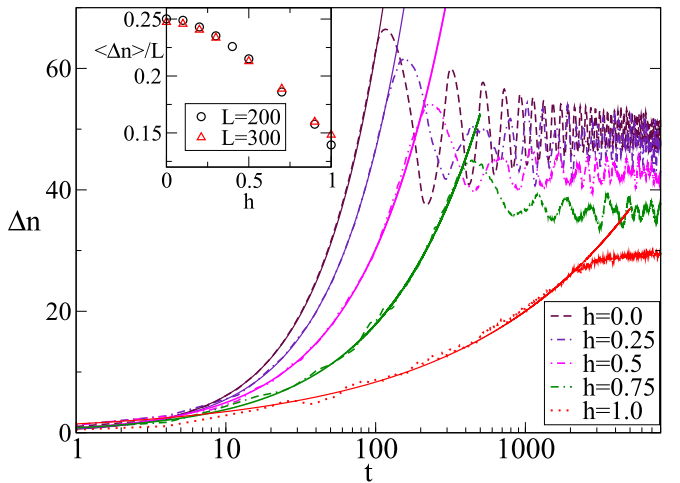


FIG. 4. (Main panel) Variation of $\delta n = \sum_i |n_i(t) - n_i(t = 0)|$ with time for different values of h and $V = 0$, and $L = 2L_A = 200$. Solid lines are $\Delta n \sim t^\gamma$ with $\gamma = 1, 0.93, 0.78, 0.67, 0.38$ for $h = 0, 0.25, 0.5, 0.75, 1$, respectively. Inset shows the variation for long time average of $\Delta n/L$ with h for $L = 200$ and 300 .

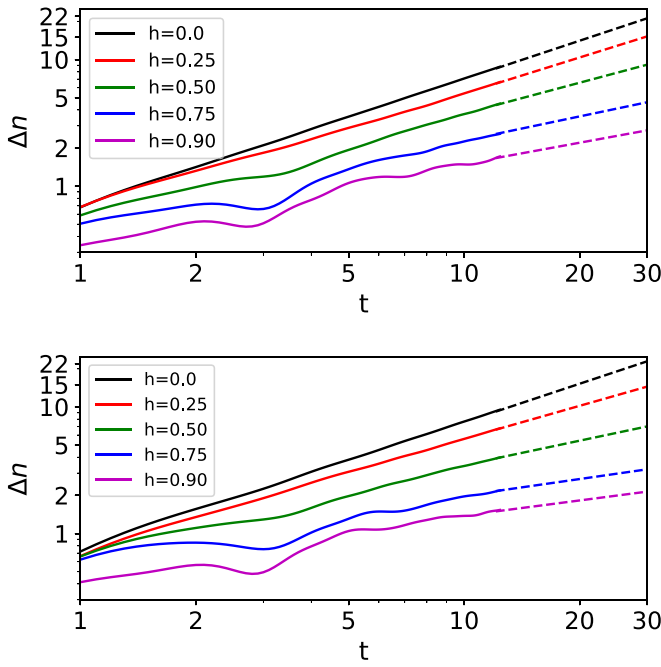


FIG. 5. Variation of $\delta n = \sum_i |n_i(t) - n_i(t=0)|$ with time for different values of h and the interaction V . Top figure shows the variation for $V = 0.5$ where solid lines are $\Delta n \sim t^\gamma$ with $\gamma = 1.00, 0.94, 0.80, 0.63, 0.55$ for $h = 0, 0.25, 0.5, 0.75, 0.90$, respectively. Bottom figure shows the variation for $V = 1.0$ where solid lines are $\Delta n \sim t^\gamma$ with $\gamma = 1.00, 0.85, 0.63, 0.43, 0.39$ for $h = 0, 0.25, 0.5, 0.75, 0.90$, respectively.

popular measures of the entanglement, i.e., von Neuman entanglement entropy. Considering a bipartition of a system in a pure state $|\psi\rangle$ into parts A and B, a standard measure of their mutual entanglement is the von Neumann entropy $S_A = -\text{Tr} \rho_A \log \rho_A$. Here ρ_A is the reduced density matrix for A, obtained after tracing part B from the full density matrix $\rho = |\psi\rangle\langle\psi|$.

We present the results for the time evolution of the entanglement entropy following the geometric quench in Fig. 7. First, we focus on the delocalized phase, i.e., $h < 1$. Both for the noninteracting case and interacting case, we find that the growth of entanglement with time obeys power-law type scaling, i.e., t^η (see Fig. 7). This exponent η seems to decrease

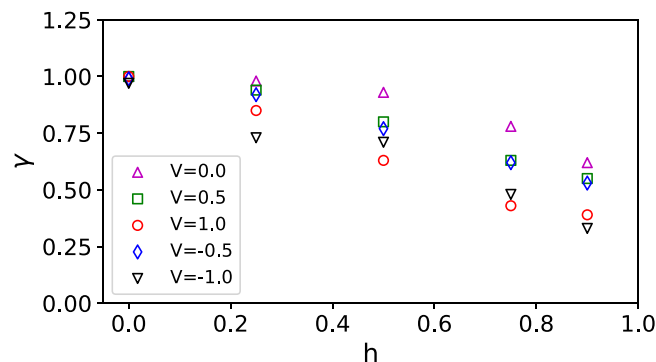


FIG. 6. Scaling exponent γ with the interaction and the disorder strength.

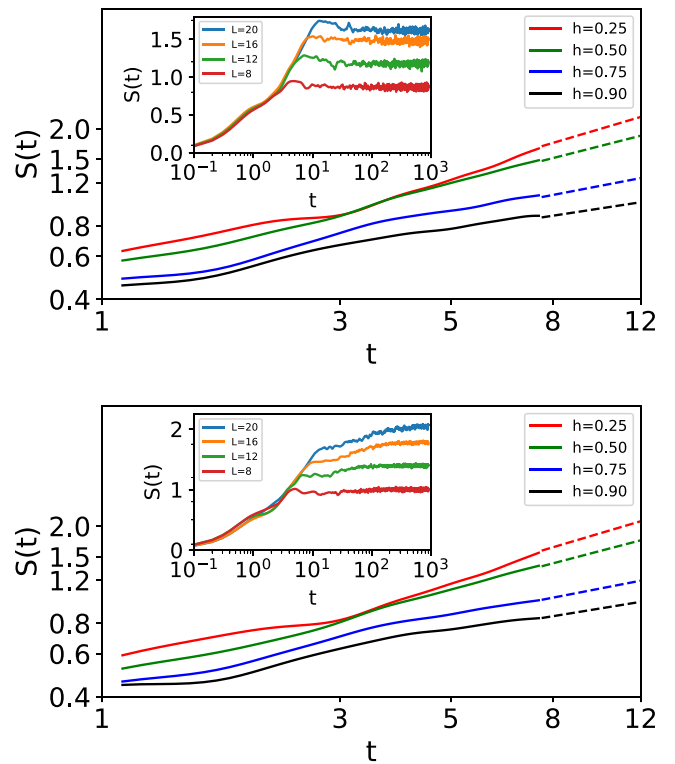


FIG. 7. Evolution of entanglement entropy in the delocalized regime. Solid lines represent actual data and dotted lines are best fit line for $S(t) \sim t^\eta$ for different values of h . Top figure shows the variation for $V = 0$ of system size $L = 32$, where $\eta = 0.60, 0.52, 0.39, 0.31$ for $h = 0.25, 0.5, 0.75, 0.90$, respectively. Inset shows the saturation of the entanglement entropy for system sizes $L = 8, 12, 16, 20$ for $h = 0.5$. Bottom figure shows the variation for $V = 0.5$ of system size $L = 32$, where $\eta = 0.61, 0.54, 0.40, 0.34$ for $h = 0.25, 0.5, 0.75, 0.90$, respectively. Inset shows the saturation of the entanglement entropy for system sizes $L = 8, 12, 16, 20$ for $h = 0.5$.

with increasing h (see Fig. 7). Note that, in the limit $h = 0$ and $V = 0$, this power-law growth of entanglement was reported in the context of geometric quench in Ref. [30]. This feature is quite unique compared to the usual global quench, where the entanglement growth is always found to be linear in time in the delocalized phase [36,50], except for long-range systems [51]. However, the long-time saturation values of entanglement entropy followed by geometric quench for delocalized phase obey volume law (see the inset of Fig. 7), which also has been observed for global quench. Now we focus on the localized phase. In the absence of interaction, the entanglement growth profile for geometric quench is very similar to the one observed for the usual global quench, i.e., there is a short time growth followed by saturation, and the saturation values do not change with the system size and hence follow area law (see Fig. 8) [37]. However, for the global quench in the presence of interaction, the time evolution profile of the entanglement entropy is very different compared to the noninteracting case. The interacting case shows a logarithmic growth followed by a saturation, while saturation values of the entanglement entropy obey volume law. On the other hand, in the case of geometric quench, we find that the entanglement

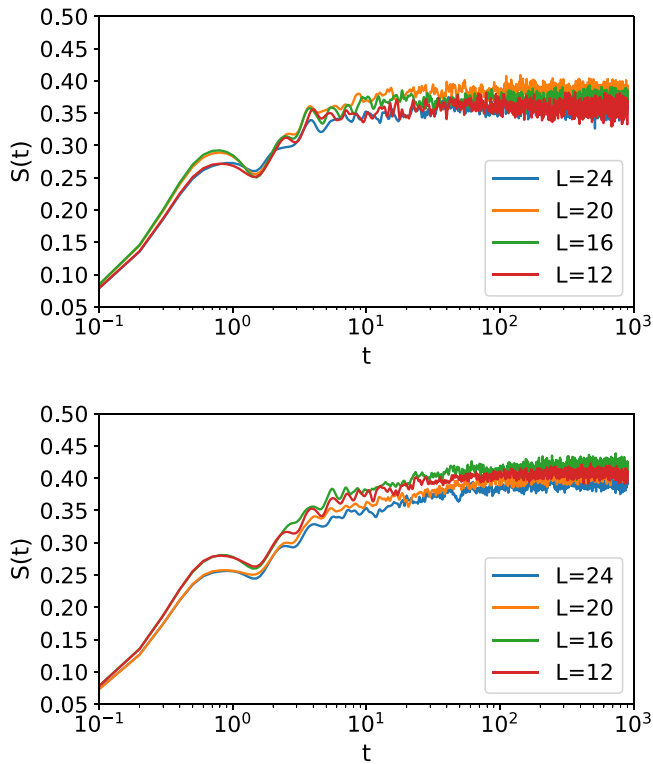


FIG. 8. Evolution of entanglement entropy in the localized region ($h = 2.0$) for $L = 12, 16, 20, 24$ for $V = 0$ (top) and $V = 0.5$ (bottom).

profile is very similar to the noninteracting results. The time evolution profile of the entanglement entropy does not possess a logarithmic growth; also the saturation value obeys area law (see Fig. 8). This area law can also be understood from the long time site-occupation profile, where we found that the wave front almost gets frozen and the site occupation goes exponentially to zero on the new sites independent of the system size. Hence it is expected that the long time dynamics of the bipartite entanglement entropy would not depend on the system size; that automatically implies the long time saturation value would obey area law. We have also checked the robustness of our results by repeating our calculations for different initial states (see the Appendix).

V. CONCLUSIONS

In this work, our main goal was to understand the effect of geometric quench on localized and delocalized phases. While there have been extensive studies on such systems, global quench has been used as a very important tool both experimentally [15–17] and theoretically to characterize these phases; the effect of geometric quench has not been well explored so far. We use mainly two types of diagnostics: (1) site-occupation profile and (2) entanglement entropy. While entanglement entropy is a very popular measure to detect localization-delocalization transition even when a system undergoes a global quench, site-occupation profile remains a useful tool for geometric quench. We have extensively studied the effect of the incommensurate potential strength and the interaction strength on the wave front velocities. We found

that, in the delocalized phase, the wave front moves towards the boundary, but, in the localized phase (even in the presence of interactions), the wave front almost gets frozen, i.e., almost no change can be observed even when one waits a very long time.

On the other hand, the entanglement entropy shows quite a distinct feature compared to the global quench. In the delocalized phase, the entanglement growth is t^η with $\eta < 1$, in contrast to the linear growth found in the case of global quench. However, the saturation values are observed to be obeying a volume law, i.e., the same as the global quench. Recently it has been observed that the entanglement entropy for a bipartition which is already close to maximally entangled can only grow very little and due to the monogamy of entanglement [52,53], in order to generate entanglement across the cut, highly nontrivial processes have to occur to free some degrees of freedom before they can entangle with the other subsystem [54]. Given that our initial state is the ground state of a Hamiltonian on lattice size L_A , it has entanglement built into that subsystem. On the other hand, the usual product random states (e.g., Néel state) have zero entanglements in each subsystem. Hence one might expect that entanglement growth for the random product state is much faster, i.e., linear in time, compared to t^η growth with $\eta < 1$ for our case.

In the localized phase, the entanglement profile for the geometric quench cannot be distinguished between Anderson localized phase and the MBL phase. In both cases, the saturation values obey area law. These results can be understood from the wave front dynamics, where we find that the wave front almost gets frozen and the site occupation goes exponentially to zero on the new sites. The decay length scale is independent of the system size (it depends on the single-particle localization length) [55]. Given that one expects the bipartite entanglement entropy will depend on the site occupations on the empty sites, it is expected that the entanglement dynamics would not depend on the system size.

Given that the geometric quench can be experimentally realized in an ultracold setup [33,34], our future plan will be to investigate similar protocols for long-range systems [51,56] and systems with single-particle mobility edges [57]. Also, it will be interesting to study non-Hermitian [58] systems in the shade of similar light.

ACKNOWLEDGMENTS

R.M. acknowledges the DST-Inspire fellowship by the Department of Science and Technology, Government of India, and SERB start-up grant (No. SRG/2021/002152) for their support. The support and the resources provided by “PARAM Shivay Facility” under the National Supercomputing Mission, Government of India at the Indian Institute of Technology Varanasi, are gratefully acknowledged.

APPENDIX

In the main text, we had presented the results of the entanglement dynamics for geometric quench starting from an initial state $|\psi(t=0)\rangle = |GS\rangle_{L_A} \otimes |0\rangle_{(L-L_A)}$. We found that, in contrast to the global quench, the saturation of entanglement entropy in the MBL phase due to the geometric quench

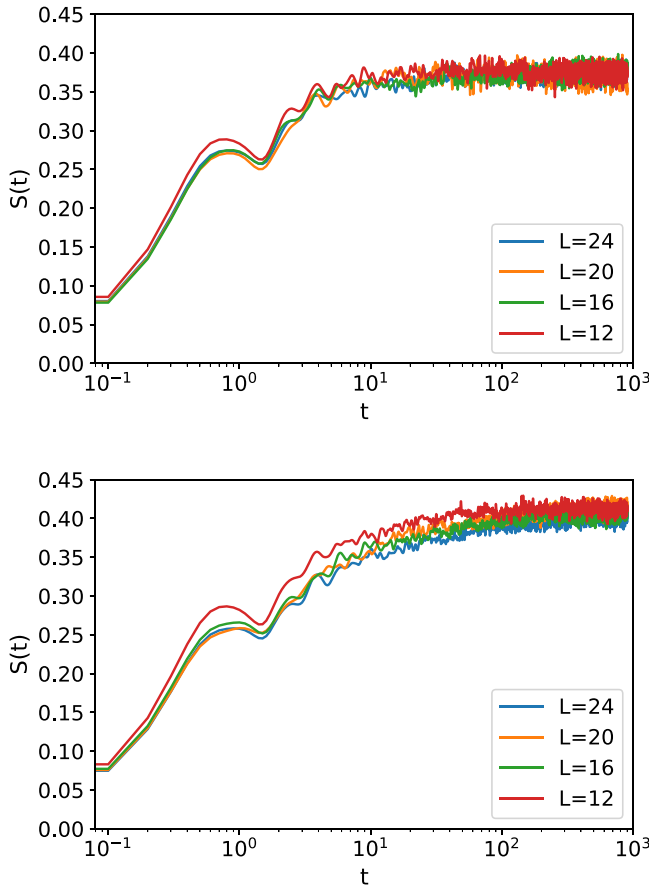


FIG. 9. Evolution of entanglement entropy in the localized region ($h = 2.0$) for the first excited state ($|\psi_1\rangle$) as initial state. Top figure shows the variation for $V = 0.0$ for system sizes $L = 12, 16, 20, 24$. Bottom figure shows the variation for $V = 0.5$ for system sizes $L = 12, 16, 20, 24$.

obeys area law, while, in the global quench, it obeys volume law. In order to check the robustness of our results, we now repeat our calculation for initial states,

$$|\psi_1(t=0)\rangle = |E_1\rangle_{L_A} \otimes |0\rangle_{(L-L_A)}, \quad (\text{A1})$$

$$|\psi_2(t=0)\rangle = |E_2\rangle_{L_A} \otimes |0\rangle_{(L-L_A)}, \quad (\text{A2})$$

where $|E_1\rangle$ and $|E_2\rangle$ are respectively the first and second excited states of the Hamiltonian $H(L_A)$.

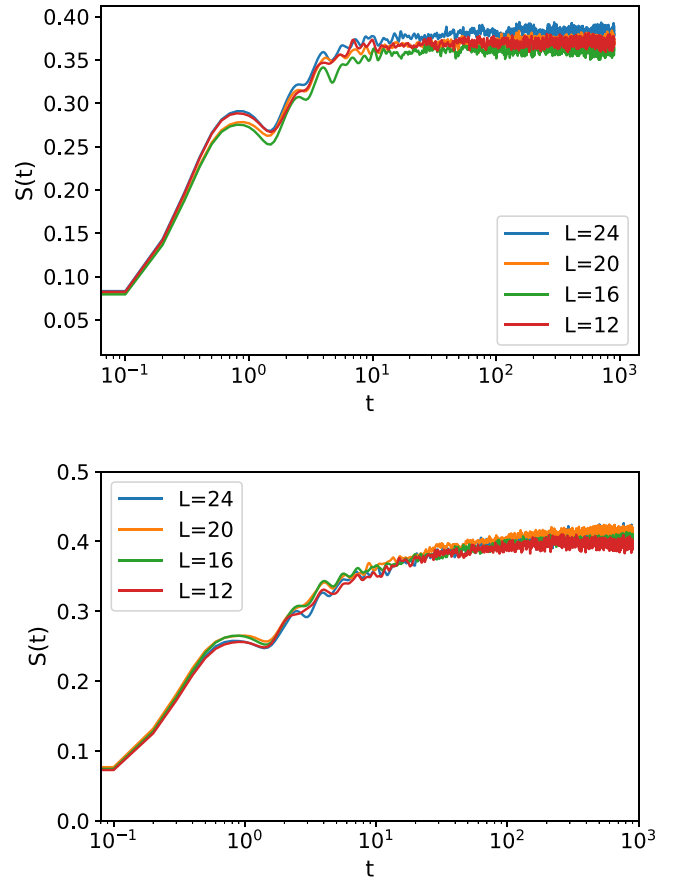


FIG. 10. Evolution of entanglement entropy in the localized region ($h = 2.0$) for the second excited state ($|\psi_2\rangle$) as initial state. Top figure shows the variation for $V = 0.0$ for system sizes $L = 12, 16, 20, 24$. Bottom figure shows the variation for $V = 0.5$ for system sizes $L = 12, 16, 20, 24$.

In Fig. 9 and Fig. 10, we show the entanglement growth for the initial states $|\psi_1\rangle$ and $|\psi_2\rangle$. In both cases, we found that, for $V = 0$ (in the Anderson-localized phase) and $V = 0.5$ (in the MBL phase), the entanglement entropy saturates to a value that does not depend on the system size L , which corresponds to area law. While for $V = 0$ in the Anderson-localized phase, the saturation value of the entanglement entropy followed by a global quench also satisfies area law, but, for the nonzero value of V (in the MBL phase), it is extensive.

-
- [1] P. Anderson, *Phys. Rev.* **109**, 1492 (1958).
[2] E. Abrahams, P. W. Anderson, D. C. Licciardello, and T. V. Ramakrishnan, *Phys. Rev. Lett.* **42**, 673 (1979).
[3] D. Basko, I. Aleiner, and B. Altshuler, *Ann. Phys. (NY)* **321**, 1126 (2006).
[4] J. A. Kjäll, J. H. Bardarson, and F. Pollmann, *Phys. Rev. Lett.* **113**, 107204 (2014).
[5] T. Devakul and R. R. P. Singh, *Phys. Rev. Lett.* **115**, 187201 (2015).
[6] D. J. Luitz, N. Laflorencie, and F. Alet, *Phys. Rev. B* **91**, 081103(R) (2015).
[7] C. L. Bertrand and A. M. García-García, *Phys. Rev. B* **94**, 144201 (2016).
[8] M. Serbyn and J. E. Moore, *Phys. Rev. B* **93**, 041424(R) (2016).
[9] D. J. Luitz, *Phys. Rev. B* **93**, 134201 (2016).
[10] X. Yu, D. J. Luitz, and B. K. Clark, *Phys. Rev. B* **94**, 184202 (2016).
[11] Y. Prasad and A. Garg, [arXiv:2202.05217](https://arxiv.org/abs/2202.05217).
[12] V. Khemani, S. P. Lim, D. N. Sheng, and D. A. Huse, *Phys. Rev. X* **7**, 021013 (2017).
[13] V. Khemani, D. N. Sheng, and D. A. Huse, *Phys. Rev. Lett.* **119**, 075702 (2017).

- [14] J. Šuntajs, J. Bonča, T. Prosen, and L. Vidmar, *Phys. Rev. B* **102**, 064207(R) (2020).
- [15] M. Schreiber, S. S. Hodgman, P. Bordia, H. P. Lüschen, M. H. Fischer, R. Vosk, E. Altman, U. Schneider, and I. Bloch, *Science* **349**, 842 (2015).
- [16] S. S. Kondov, W. R. McGehee, W. Xu, and B. DeMarco, *Phys. Rev. Lett.* **114**, 083002 (2015).
- [17] J. Smith, A. Lee, P. Richerme, B. Neyenhuis, P. W. Hess, P. Hauke, M. Heyl, D. A. Huse, and C. Monroe, *Nat. Phys.* **12**, 907 (2016).
- [18] J. M. Deutsch, *Phys. Rev. A* **43**, 2046 (1991).
- [19] M. Srednicki, *Phys. Rev. E* **50**, 888 (1994).
- [20] M. Rigol, V. Dunjko, and M. Olshanii, *Nature (London)* **452**, 854 (2008).
- [21] V. Oganesyan and D. A. Huse, *Phys. Rev. B* **75**, 155111 (2007).
- [22] A. Pal and D. A. Huse, *Phys. Rev. B* **82**, 174411 (2010).
- [23] C. Holzhey, F. Larsen, and F. Wilczek, *Nucl. Phys. B* **424**, 443 (1994).
- [24] G. Vidal, J. I. Latorre, E. Rico, and A. Kitaev, *Phys. Rev. Lett.* **90**, 227902 (2003).
- [25] J. I. Latorre, E. Rico, and G. Vidal, *Quantum Inf. Comput.* **4**, 048 (2004).
- [26] P. Calabrese and J. Cardy, *J. Stat. Mech.* (2004) P06002.
- [27] L. Amico, R. Fazio, A. Osterloh, and V. Vedral, *Rev. Mod. Phys.* **80**, 517 (2008).
- [28] P. Calabrese, J. Cardy, and B. Doyon, *J. Phys. A: Math. Theor.* **42**, 500301 (2009).
- [29] J. Mossel, G. Palacios, and J.-S. Caux, *J. Stat. Mech.* (2010) L09001.
- [30] V. Alba and F. Heidrich-Meisner, *Phys. Rev. B* **90**, 075144 (2014).
- [31] R. Modak, L. Vidmar, and M. Rigol, *Phys. Rev. E* **96**, 042155 (2017).
- [32] L. Vidmar, D. Iyer, and M. Rigol, *Phys. Rev. X* **7**, 021012 (2017).
- [33] U. Schneider, L. Hackermüller, J. P. Ronzheimer, S. Will, S. Braun, T. Best, I. Bloch, E. Demler, S. Mandt, D. Rasch, and A. Rosch, *Nat. Phys.* **8**, 213 (2012).
- [34] J. P. Ronzheimer, M. Schreiber, S. Braun, S. S. Hodgman, S. Langer, I. P. McCulloch, F. Heidrich-Meisner, I. Bloch, and U. Schneider, *Phys. Rev. Lett.* **110**, 205301 (2013).
- [35] S. Aubry and G. André, *Ann. Israel Phys. Soc.* **3**, 133 (1980).
- [36] S. Iyer, V. Oganesyan, G. Refael, and D. A. Huse, *Phys. Rev. B* **87**, 134202 (2013).
- [37] J. H. Bardarson, F. Pollmann, and J. E. Moore, *Phys. Rev. Lett.* **109**, 017202 (2012).
- [38] P. Calabrese and J. Cardy, *J. Stat. Mech.* (2007) P10004.
- [39] J. M. Stephan and J. Dubail, *J. Stat. Mech.* (2011) P08019.
- [40] V. Eisler and I. Peschel, *J. Stat. Mech.* (2007) P06005.
- [41] V. Eisler, D. Karevski, T. Platini, and I. Peschel, *J. Stat. Mech.* (2008) P01023.
- [42] M. Rigol, *Phys. Rev. A* **72**, 063607 (2005).
- [43] S. R. White, *Phys. Rev. Lett.* **69**, 2863 (1992).
- [44] A. J. Daley, C. Kollath, U. Schollöck, and G. Vidal, *J. Stat. Mech.: Theor. Exp.* (2004) P04005.
- [45] U. Schollwöck, *Ann. Phys. (NY)* **326**, 96 (2011).
- [46] G. Vidal, *Phys. Rev. Lett.* **93**, 040502 (2004).
- [47] Fishman, White, and Stoudenmire, The ITensor Software Library for Tensor Network Calculations, 2020.
- [48] T. Sabetta and G. Misguich, *Phys. Rev. B* **88**, 245114 (2013).
- [49] V. Eisler and Z. Rácz, *Phys. Rev. Lett.* **110**, 060602 (2013).
- [50] H. Kim and D. A. Huse, *Phys. Rev. Lett.* **111**, 127205 (2013).
- [51] R. Modak, and T. Nag, *Phys. Rev. Research* **2**, 012074(R) (2020).
- [52] V. Coffman, J. Kundu, and W. K. Wootters, *Phys. Rev. A* **61**, 052306 (2000).
- [53] T. J. Osborne and F. Verstraete, *Phys. Rev. Lett.* **96**, 220503 (2006).
- [54] T. L. M. Lezama and D. J. Luitz, *Phys. Rev. Research* **1**, 033067 (2019).
- [55] J. Hauschild, F. Heidrich-Meisner, and F. Pollmann, *Phys. Rev. B* **94**, 161109(R) (2016).
- [56] R. Modak and T. Nag, *Phys. Rev. E* **101**, 052108 (2020).
- [57] R. Modak, S. Ghosh, and S. Mukerjee, *Phys. Rev. B* **97**, 104204 (2018).
- [58] R. Modak and B. P. Mandal, *Phys. Rev. A* **103**, 062416 (2021).